Simulation of birdfoot delta formation with application to the Mississippi Delta

H. J. Seybold,[1] P. Molnar,[2] H. M. Singer,[1] J. S. Andrade Jr.,[1,3] H. J. Herrmann,[1,3] and W. Kinzelbach[2]

Received 5 January 2009; revised 28 April 2009; accepted 14 May 2009; published 22 August 2009.

[1] Recently, Seybold et al. (2007) proposed a reduced complexity model which simulates the process of delta formation on geological time scales. It includes subaerial and subaqueous growth in a three-dimensional framework. In this paper we apply this model to the formation of a river-dominated delta and compare the model dynamics with observations of the formation of the Balize Lobe of the Mississippi River Delta. The model generates both subaerial and subaqueous channels and lateral levee formations as well as a profile morphology with steep drop-offs and a flat delta surface which is similar to natural ones. We show that the dimensionless parameters of the model may be consistently rescaled to match the Balize Lobe. This means that after rescaling the water flows, the subaerial geometry and time, the deposited (subaqueous) lobe volume, the sediment and water flows, the age, as well as the sediment capture ratio match the observed data. Finally, we use detrended fluctuation analysis to show that the modeled long-term dynamics of the delta formation process shows a complex temporal correlation structure. A characteristic time scale separates periods of consistent delta growth by gradual sediment deposition at the mouths of distributary channels from periods during which random large-scale channel avulsions lead to rapid change and the formation of new channels and subaqueous-dominated deposition.

Citation: Seybold, H. J., P. Molnar, H. M. Singer, J. S. Andrade Jr., H. J. Herrmann, and W. Kinzelbach (2009), Simulation of birdfoot delta formation with application to the Mississippi Delta, *J. Geophys. Res.*, *114*, F03012, doi:10.1029/2009JF001248.

1. Introduction

[2] How river deltas emerge and how they evolve are classic questions in geomorphology [*Bates*, 1953; *Coleman and Gagliano*, 1964; *Wright and Coleman*, 1973; *Galloway*, 1975; *Orton and Reading*, 1993]. Coastal deltas are morphologically very active sedimentary landforms where strong deposition caused by the high sediment supply from the river is competing with reworking wave and current action. The deposition of coarse sediment at the mouth of the delta is often accompanied by the formation of oil and coal reservoirs [*Morgan*, 1977; *Coleman*, 1975; *Coleman and Prior*, 1980; *Allen et al.*, 1981]. As a result, the first field studies investigating the geological structure of coastal deltas were carried out early in the 20th century primarily by oil companies, for example in the Mississippi Delta [*Fisk*, 1947, 1952; *Kolb and van Lopik*, 1958; *Coleman and Gagliano*, 1964, 1965]. Today the gulf of Mexico at the mouth of the Mississippi is one of the major offshore oil fields in the United States. The understanding of the facies, relationships and mechanisms responsible for the development and distribution of deltaic deposits therefore is essential for efficient exploration and oil extraction [*Bates*, 1953; *Coleman and Prior*, 1980]. Six major lobes of the Mississippi Delta have been identified and their ages have been determined using radiocarbon dating [*Fisk and McFarlen*, 1955; *McFarlen*, 1961; *Saucier*, 1963; *Frazier*, 1967; *Törnqvist et al.*, 1996]. More recent studies have shown that, beside the major lobes, there are also three to six sublobes [*Penland et al.*, 1987]. The main lobes of the delta are shown in Figure 1.

[3] In recent years the study of changes in deltaic topography has come into focus because of coastal land loss related to the rising sea level combined with extreme weather events causing significant damage. Coastal hazards have an immense economic impact as 25% of the world's population live on deltaic coastlines and wetlands [*Giosan and Bhattacharya*, 2005; *Syvitski et al.*, 2005]. To obtain a deeper understanding of the dynamic processes involved in delta formation, laboratory experiments have been set up in recent years in order to quantify sedimentation and erosion processes in a delta. Experiments have been carried out with some success in the "eXperimental EarthScape" (XES) facility of the St. Anthony Falls Laboratory [*Kim et al.*, 2006; *Swenson et al.*, 2005; *Paola et al.*, 2001; *Sheets et al.*, 2002]. Other recent laboratory experiments have shown that the cohesion of the sediment transported by the stream is an essential factor in the formation of elongated birdfoot deltas

[1] Computational Physics for Engineering Materials, Institute for Building Materials, ETH Zurich, Zurich, Switzerland.
[2] Institute of Environmental Engineering, ETH Zurich, Zurich, Switzerland.
[3] Departamento de Física, Universidade Federal do Ceará, Ceará, Brazil.

0148-0227/09/2009JF001248

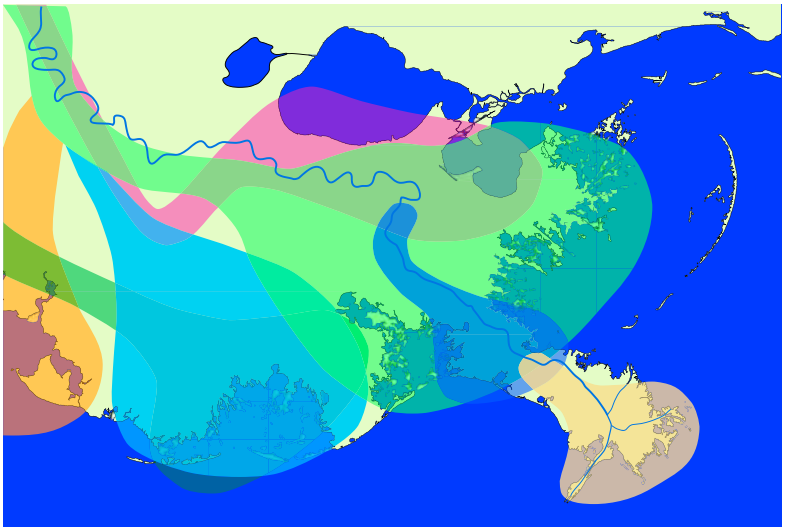

Figure 1. Main lobes of the Mississippi. The currently active Balize Lobe is marked in cream; the other lobes are Sale Cypremort (>4600 B.C., orange), Cocodrie (4600–3500 B.C., violet), Teche (3500–2800 B.C., dark green), St. Bernard (2800–1000 B.C., light green), Lafourche (1000–300 B.C., light blue), and the Plaquemine delta lobe (750–300 B.C., dark blue). After *Coleman* [1975] and *Kolb and van Lopik* [1958].

such as the Mississippi. Because of the cohesion of the sediment, the channel beds are stabilized which leads to more distinct channel patterns and lower channel migration. In nature this channelization happens because of riparian vegetation which stabilizes the bed at the river banks and bars [*Hoyal and Sheets*, 2009].

[4] Although the techniques for topographic measurements and experimental setups have advanced considerably, computational modeling of deltas has proven to be very difficult as the systems are highly complex and large time scales have to be taken into account. Physically based models generally combine hydrodynamics derived from the Navier-Stokes equations with an empirical sediment transport law based on bottom shear stress and sediment continuity. This set of partial differential equations is then integrated using finite element or finite volume techniques. Fully three-dimensional simulations with hydrodynamic-topographic coupling have been carried out by *Harris et al.* [2005] using ECOM-SED and by *Edmonds and Slingerland* [2007, 2008], who applied the Delft-3D model to study the mechanics of river mouth bar formation. Although the models based on partial differential equations describe the details of the flow, numerical simulations of realistic river basins and delta formation over geological times are far beyond today's computational power. Usually these models cover only small sections of some kilometers over several months or years.

[5] In contrast, our knowledge of the topography and channel dynamics is derived from digital elevation model (DEM) data and sediment records covering scales of broadly $10^0 - 10^6$ m and $10^{-1} - 10^5$ years. Process models are required that include the changing boundary conditions governing land-surface changes and mass fluxes over these scales [*Brasington and Richards*, 2007]. While for the very small and very large scales well-developed models exist, the mesoscale is still not yet well understood [*Wolinsky*, 2009]. Thus the challenge of geomorphological modeling is to reduce the complexity of the microscopic physical equations without modifying the characteristic mesoscopic behavior of the system [*Coulthard*, 2001]. During recent years "reduced complexity models" (RCMs) based on the idea of cellular automata [*Wolfram*, 2002] have proven to be very successful in modeling the time evolution of geophysical processes [e.g., *Paola et al.*, 2001; *Coulthard et al.*, 2007]. The motivation for this type of modeling is not to simulate the detailed evolution of a given river, but to identify the essential physics of the underlying processes [*Murray*, 2003]. The results of these simulations then can be compared and validated with appropriate coarse-grained field measurements and laboratory experiments. Recent advances in this field have sought to achieve these ends through the development of novel cellular discretization methods efficiently describing the evolution of the topography combined with an increasing reliance on high-quality topographic data [*Brasington and Richards*, 2007; D. Divins and D. Metzger, NGDC Coastal Relief Model, Central Gulf of Mexico Grids, 2006, http://www.ngdc.noaa.gov/mgg/coastal/coastal.html (hereinafter referred to as Divins and Metzger, 2006)]. RCMs are based on simplified equations that still capture the essential morphodynamics of the landscape changing processes. These simplifications introduce a new set of problems as the model equations are often based on empirical descriptions instead of previously well-understood physical properties and variables. Additional complications then emerge because of the fact that the nature of these new parameterizations may themselves be both scale and grid dependent and not easily transferable to real scales [*Brasington and Richards*, 2007; *Murray*, 2003, 2007]. The work of Murray and Paola on braided river streams [*Murray and Paola*, 1994] is often considered as the seminal work in applying RCMs in geomorphology. Other more recent examples are CEASAR [*Coulthard et al.*, 1998] and EROS [*Davy and Crave*, 2000] for river channel dynamics and alluvial sediment transport or LISFLOOD

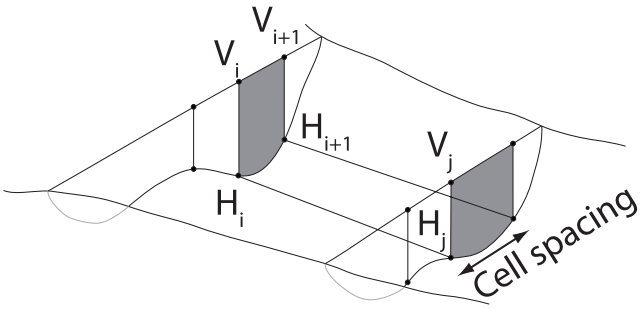

Figure 2. Sketch of a cross section through a channel segment and how the water level V_i and topography H_i are related to calculate the hydraulic conductivity. The hydraulic conductivity can be interpreted as the average water depth on the channel segment between two neighboring nodes. The total channel width is variable and determined exclusively by the flow conditions. Normally a channel is several cells wide, and flow can be laterally exchanged among the cells.

[*van der Knijff and de Roo*, 2008] for modeling flood plain dynamics. Reduced complexity models have also been applied to delta formation by *Sun et al.* [2002]. This model is completely topography driven and does not account for subaqueous sediment transport at the delta front or backwater and overbank effects. Other models like the two-dimensional DELTASIM [*Hoogendoorn and Weltje*, 2006] include subaqueous sedimentation, but lack the description of lateral sediment transport. A comparison and discussion of the different models and strategies are given by *Overeem et al.* [2005].

[6] On the basis of RCM ideas, *Seybold et al.* [2007] presented a new model to simulate the time evolution and formation of river deltas. This model combines the simplicity of the cellular models with the essential hydrodynamic features necessary to reproduce realistic river delta patterns, which cannot be obtained by classical topography driven flow equations such as Manning-Strickler. The model describes a subaerial and subaqueous growth of the deltaic deposits using a simple hydrodynamic routing with an explicit water surface coupled to the topography by an erosion and deposition law. By modifying the erosion-deposition law, the model reproduces the formation of the Galloway [*Galloway*, 1975] end-member delta types, namely, river-, wave- and tide-dominated. Furthermore several characteristics of the time behavior of real delta formation such as lobe switching could be observed [*Seybold et al.*, 2007].

[7] In this paper we apply the model to the case of a river-dominated delta and focus on the specific static and dynamic features of this delta type. We compare the model dynamics with that of the Balize Lobe of the Mississippi Delta and show that the model captures the key features of the delta formation process, such as the self organized formation of subaerial and subaqueous natural levees. We investigate the simulated delta evolution and the internal behavior of the model by comparing the model parameters with measured data obtained for the Mississippi. Our aim is to show that the model is internally logical and gives physically meaningful results, that the dimensionless parameters may be rescaled consistently to fit observations, and that the model produces long-term simulated dynamics of the delta formation process with a complex temporal correlation structure.

[8] The paper is organized as follows: in section 2 we present a description of the model implementation and the details of the model equations, followed by section 3, which summarizes the model parameters used for the simulation of the birdfoot delta lobe. The simulated delta dynamics and the consistency of the RCM equations are checked by comparing the simulation results with data from the Mississippi. In section 5 we investigate the simulated long-term dynamics of the delta growth.

2. Model

[9] The landscape is discretized on a regular square grid with fixed spacing, where each node is connected by bonds to its four closest neighbors. The elevation of the topography H_i and the water surface V_i are defined on the nodes. On the bonds between two neighboring nodes i and j, the hydraulic conductivity for the water flow from node i to node j is given by

$$\sigma_{ij} = c_\sigma \begin{cases} \dfrac{V_i + V_j}{2} - \dfrac{H_i + H_j}{2} & \text{if } > 0 \\ 0 & \text{if } \le 0. \end{cases} \tag{1}$$

The hydraulic conductivity can be interpreted as the average depth of the water in a channel segment; if the channel is deep, more water can be transported than in a shallow one. A sketch of a distributary channel segment is shown in Figure 2. The model considers only surface water flow, thus the hydraulic conductivity is also set to zero if the water level in the source node of the flow is below the surface. The water is routed downhill because of a hydrostatic pressure gradient which induces a flow I_{ij} between nodes i and j as

$$I_{ij} = \sigma_{ij}\left(V_i - V_j\right). \tag{2}$$

This equation implies a nonlinear relation between the discharge I_{ij} and the water level V_i as σ_{ij} is itself a function of of V_i, namely, $\sigma_{ij} = \sigma_{ij}(V_i,V_j)$.

[10] The change of the topography takes place on a much longer time scale than the hydrodynamic nature of the flow, which means that the water flux can be assumed to be in a quasi steady state regime. The conservation of the water mass is given by the continuity of flows I_{ij} entering and leaving node i,

$$\sum_j I_{ij} = 0. \tag{3}$$

where the sum runs over all neighbors connected to node i.

[11] The resulting system of equations (1)–(3) is solved using a relaxation method. Boundary conditions are needed to close the system. On the sea side Dirichlet boundary conditions are applied with a fixed water level, while inflow boundaries and no-flow lateral boundaries are applied on the land. Water and sediment are injected into the domain by defining inputs of water I_0 and sediment J_0 at an entrance

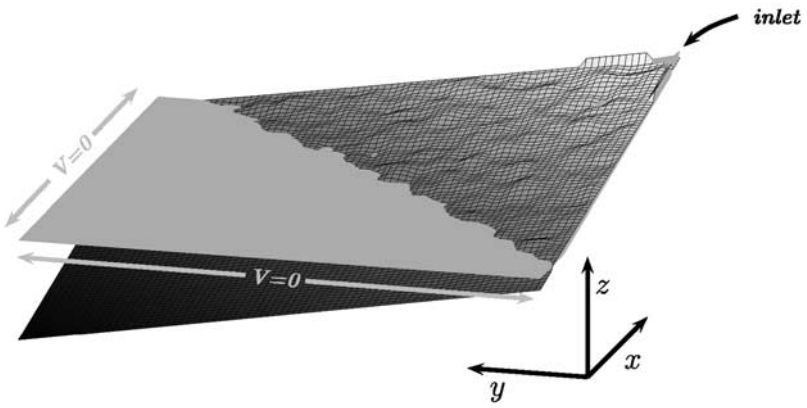

Figure 3. Sketch of the initial and boundary conditions for the simulation with the river delta model [*Seybold et al.*, 2007]. Water and sediment currents are injected at the upper node (inlet), and the water levels on the sea boundaries are kept constant ($V = 0$). The landscape is initialized as an inclined plane with a superimposed disordered topography. The water surface (light gray) is parallel to the horizontal xy plane.

inlet node (see Figure 3). The landscape is initialized with a given water level below the ground and runoff is produced when the water level exceeds the surface.

[12] The sedimentation/erosion rate dS_{ij} is modeled by a phenomenological relation. We use a simplified law with a common constant for erosion and deposition. In the case of river-dominated deltas it is dependent only on the magnitude of the flow I_{ij}. Thus equation (5) of *Seybold et al.* [2007] reduces to

$$dS_{ij} = c\left(I^{\star} - |I_{ij}|\right), \tag{4}$$

where $I^{\star}$ is the threshold for the water flow which determines whether there is erosion or deposition between nodes i and j. If $dS_{ij} > 0$ we have deposition and if $dS_{ij} < 0$ we are in the erosive regime. The sedimentation rate dS_{ij} computed by (4) is a potential rate, the actual rate $dS^{\star}_{ij}$ is limited by the supply of sediment through the sediment discharge J_{ij}. Thus if $dS_{ij} > J_{ij}$ all sediment is deposited on the surface and J_{ij} is set to zero. In the other cases J_{ij} is reduced by the sedimentation rate or increased in the case of erosion, respectively.

[13] We also introduce an erosion threshold for numerical stability reasons, so if the potential rate dS_{ij} is smaller than a given value θ then we do not allow erosion locally in that time step. This condition occurs very rarely in the simulation. As $|I_{ij}| \rightarrow 0$ we get the deposition capacity

$$dS_{\max} = cI^{\star} \tag{5}$$

[14] In summary we have the following situation

$$dS^{\star}_{ij} = \begin{cases} dS_{ij}, & J'_{ij} = J_{ij} - dS_{ij} \quad \text{if} \quad \theta < dS_{ij} < J_{ij} \\ J_{ij}, & J'_{ij} = 0 \quad \text{if} \quad dS_{ij} > J_{ij} \\ 0\ , & J'_{ij} = J_{ij} \quad \text{if} \quad dS_{ij} < \theta \end{cases} \tag{6}$$

where J_{ij} are the sediment transport rates before and J'_{ij} after the sedimentation time step.

[15] The parameter c modulates how much sediment can be eroded or deposited. The fact that the parameter c is identical for erosion and deposition is a limitation of the model because it has to capture the effect of both processes. In the erosion mode, c represents the erodibility of the surface, sediment size, etc., while in the deposition mode, c primarily represents the settling velocity of the suspended particles and the trapping efficiency in a bond in relation to the flow. For simplicity the model does not distinguish bed load and suspended load and also sediment grain size effects are not considered. The landscape is modified according to

$$H'_i = H_i + \frac{\Delta t}{2} dS^{\star}_{ij} \tag{7}$$

$$H'_j = H_j + \frac{\Delta t}{2} dS^{\star}_{ij}, \tag{8}$$

where the sediment is deposited equally on both ends of the bond.

[16] The equations hold for both erosion and deposition and ensure sediment continuity (Exner's equation) because the change of the landscape in Δt is given by $(H'_i - H_i)/\Delta t = 1/2 dS^{\star}_{ij}$ where $dS^{\star}_{ij}$ is exactly the change of the sediment flux through node i.

[17] Subaqueous water currents tend to smooth out steep gradient changes. This is modeled by a Laplacian filter which smears out hard edges and corners

$$H'_i = (1 - \epsilon) H_i + \frac{\epsilon}{4} \sum_{N.N.} H_j, \quad \text{if} V_i > H_i \tag{9}$$

using the elevations of the nearest neighbors which are connected to H_i in the lattice grid. The remaining sediment is advected by the water outflows

$$J^{out}_{ij} = \frac{\sum_k J^{in}_{ik}}{\sum_k |I^{out}_{ik}|} I_{ij}, \tag{10}$$

where the upper sum runs over all inflowing sediment and the lower one over the water outflows. Note that at the

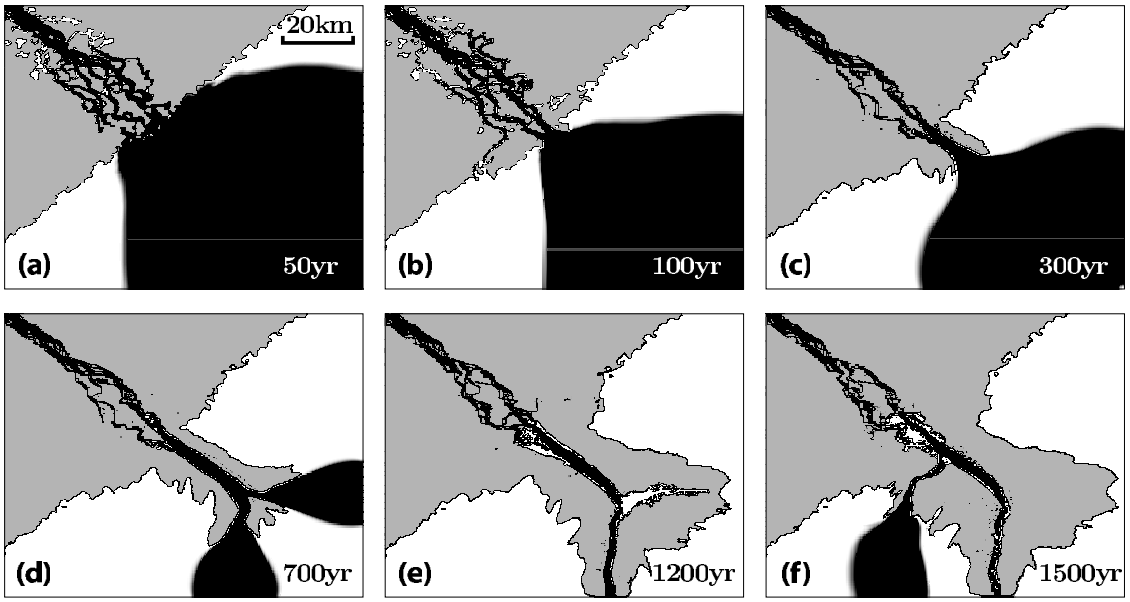

Figure 4. The time evolution of a birdfoot delta. (a) The coastline of the delta after 50 years is drawn and shows the initial stage of the delta formation. (b) Between 50 years and 100 years the delta mainly deposits along the coast, while (c) after 300 years the main channel progrades into the sea, depositing sediment mainly on its levee sides. (d) After 700 years the main channel splits into two distributaries, where (e) the smaller one becomes inactive after 1200 years. (f) A new channel breaks through the sidewalls after 1500 years. The area of active sediment transport is marked in black. Here one can see how sediment flux emerges in new channels that are abandoned later.

boundary, sediment which is not deposited before reaching the boundary exits the domain together with the water flux. Iterating the equations (1)–(10) determines the time evolution of the system. The time step Δt refers to the erosion-sedimentation process. Within this time step the water flow I_{ij} is assumed to be in steady state.

3. Simulation

[18] The system was initialized on a 279 × 279 lattice with a parabolic valley where the main slope runs downhill along the diagonal of the lattice. Below the sea the landscape is planar with a constant slope $s > 0$. Furthermore we assume that the initial landscape has a disordered topography by adding small uniformly distributed noise to H_i (see Figure 3). The elevation change due to the noise is of the order of 1% compared to the total height difference between the highest and lowest point of the simulation domain. The initial water table at the bottom of the valley was set to $\delta = 0.0025$ below the surface.

[19] The unitless parameters for the water and sediment flows were chosen as $I_0 = 1.7 \times 10^{-4}$ and the sediment influx to $s_0 = 2.5 \times 10^{-4}$. The constant c_σ was chosen to be 8.5. The constant c in the erosion law is given by $c = 0.1$. The erosion threshold was set to $I^\star = 4 \times 10^{-6}$ and the maximal erosion rate was set to $\theta = -5 \times 10^{-7}$. Smoothing was applied every 24 hours with a smoothening factor $\epsilon = 1 \times 10^{-4}$. These parameters are grid size dependent and were fine-tuned to simulate the appearance of river-dominated deltas [*Seybold et al.*, 2007]. Figures 4a–4f show six snapshots of the time evolution in the simulation where we can see how the river penetrates into the sea mainly depositing its sediment along the channels forming the typical birdfoot shape. If the deposition in the main channel is too strong, the flow breaks through the channel banks and forms a new distributary channel.

4. Interpretation of the Model Parameters

[20] To compare the simulation of the model with an existing birdfoot delta we need to reinterpret and give dimensions to the model grid, parameters and variables with the observed delta size and water-sediment fluxes. We also need to verify whether the simple erosion/sedimentation law in the model equation (4) provides a meaningful process description. These are necessary tests to judge whether the model is internally consistent and provides physically correct behavior. To check if the RCM produces meaningful results we compare some easily accessible data like sediment and water fluxes and the surface pattern of a comparable delta with the simulation and rescale the simulation variables. After that the rescaled model allows us to compare other quantities from the simulation with the real case, e.g., the volume of the deposited sediment or the growth dynamics of the delta. These predictions are not trivial results of the rescaling process, because they strongly depend on the internal dynamics of the RCM and not only on the input conditions. A similar surface pattern at a given time step and correct scaled inflow/outflow conditions for the sediment do not necessarily mean that the subaqueous deposits are comparable because sediment can enter and leave the domain and is redistributed by the erosion/sedimentation rule. In this sense the comparison of the lobe deposits gives us the possibility to judge if the internal nonlinear dynamic is consistent with the processes in a real delta.

[21] We have chosen to perform the comparison on the Mississippi delta because it is the largest river-dominated delta for which we have good records of bathymetry, water and sediment discharge, and their change in time [*Keown et al.*, 1986; *Mossa*, 1996; *Corbett et al.*, 2006]. We proceed as follows: First we collect observations of water and sediment fluxes and estimate the volume of the Balize (birdfoot) Lobe of the Mississippi Delta. Second we rescale the horizontal and vertical resolution of the modeling grid, the time step and fluxes to match the observed data. Finally we interpret the form and parameters of the erosion/sedimentation law in the model to show that the model equations are internally consistent.

4.1. Water-Sediment Fluxes and Lobe Volume

[22] The Mississippi River is the largest river on the North American continent, draining more than 3.2 million km^2. Mean annual water inflow into the delta in the last century is estimated at about $\overline{Q}$ = 17000 m^3/s with rather low interannual variability [*Mossa*, 1996]. However, the sediment load delivered to the head of the delta at Tarbert Landing (31 N, 91.61 W) has been much more variable, mostly affected by relatively recent human activities. Soil conservation, sediment trapping in reservoirs and levee construction since the 1950s have led to a reduction of the suspended sediment load from about 260 to 150 Mt/a [*Keown et al.*, 1986; *Corbett et al.*, 2006; *Syvitski et al.*, 2005]. Human influence on the geomorphological processes is clearly an uncertainty for the modeling because detailed data for the presettlement times are not available. Nevertheless the influence of dam and levee construction on the Mississippi during the last 50 years, could only have affected the last 5–10% of the total formation time of the Balize Lobe. Since we are studying the development of the delta over time scales prior to human influence, we take the average annual sediment load into the delta to be $\overline{Q_s}$ = 214 Mt/a.

[23] The width of the main river at Tarbert Landing at the top of the delta is about 1000 m and it increases to about 1400 m at the Head of Passes (29.15 N, 89.25 W) where smaller channels spread onto the lobe and the continental shelf. There the bed sediment composition has changed in response to the changing sediment load toward finer fractions. We take the data from earlier surveys which give the median diameter d_{50} = 0.17 mm with 64% fine sand and 35% clay [*Keown et al.*, 1986] and we assume a mean porosity n = 0.4 (dry bulk density ρ = 1.6 t/m^3) accounting for consolidation of the sediment after it was deposited.

[24] This study is concerned with the simulation of the formation of the most recent Mississippi Delta lobe, the Balize Lobe. From geological records it is known that the Balize Lobe has been formed in the last 800–1000 years [*Draut et al.*, 2005; *Saucier*, 1994; *Roberts*, 1997]. We estimated the lobe volume with two independent methods, namely, from observations of sediment inflow and directly from bathymetric data.

[25] The first method assumes that the incoming sediment flux is constant over the entire period τ = 800–1000 years and equal to the estimated long-term mean $\overline{Q_s}$ = 214 Mt/a. When we apply this flux and assume an average porosity of n = 0.4 we get a total volumetric influx of $10.7 - 13.4 \times 10^{10}$ m^3. The study of [*Corbett et al.*, 2006] on the western flank of the Lobe has shown that approximately 40% of the delivered sediment is advected to distal regions of the shelf by current-driven resuspension and mass movements. Considering an outflow of 40% of the sediment for the Lobe area as a whole, we get an estimate of the total Lobe volume

$$V_Q = 6.4 - 8.0 \times 10^{10} m^3 \tag{11}$$

The second method uses the USGS Coastal Relief DEM (Divins and Metzger, 2006) with a resolution of 3 arc sec (cell size about 83–87 *m*) to determine the Lobe volume. First the original coastline was reconstructed from geological records using interpolation techniques. The continental shelf at the coast of southern Louisiana reaches about 50–60 *km* into the ocean, where the depth is not more than 20–50 *m*. Then it immediately drops down to a depth of several hundred to more than one thousand meters. The bathymetry of the coast-shelf transition before the formation of the Balize Lobe is obtained by using a special interpolation technique which is explained as follows: Let $H(\mathbf{x})$ be the elevation of a point $\mathbf{x}$ in the Mississippi Region at present and $\tilde{H}(\mathbf{x})$ be the landscape 1000 years before. Outside of the deposition zone we assume that the topography did not change,

$$\tilde{H}(\mathbf{x}) = H(\mathbf{x}) \qquad \forall \mathbf{x} \notin \mathcal{D}, \tag{12}$$

where $\mathcal{D}$ denotes the deposition area of the Balize Lobe (see Figure 5). The boundary of the domain $\mathcal{D}$ is fixed by the course of the ancient coastline based on *Morgan* [1977] and *Saucier* [1963] and the abyss on the sea side. The values inside the domain $\mathcal{D}$ are obtained by minimizing the slope with the boundary condition $\tilde{H}(\partial\mathcal{D}) = H(\partial\mathcal{D})$ where $\partial\mathcal{D}$ denotes the boundary of the domain $\mathcal{D}$. Assuming a smooth decay below the shore line without saddle points, a reasonable approximation of the topography in the area $\mathcal{D}$ is given by the Laplace equation

$$\nabla^2 \tilde{H} = 0 \qquad \tilde{H}(\partial\mathcal{D}) = H(\partial\mathcal{D}). \tag{13}$$

Beside providing a saddle point free interpolation which satisfies the boundary conditions, equation (13) minimizes sharp edges in the topography leading to a smooth transition between the fixed boundaries. Furthermore it minimizes the potential energy of the surface, which means that the sediment lies at its lowest possible elevation with respect to the given boundary conditions.

[26] For solving the equation numerically we used a successive overrelaxation scheme (SOR) directly on the numerical data grid provided by the DEM to solve (13) for $\tilde{H}$. Convergence was defined for a total residual of less than 10^{-15}. The volume of the Lobe deposit is then computed as the difference between the DEM of the Lobe surface and the interpolated original surface which yields a total volume

$$V_D = 8.7 - 9.3 \times 10^{10} m^3. \tag{14}$$

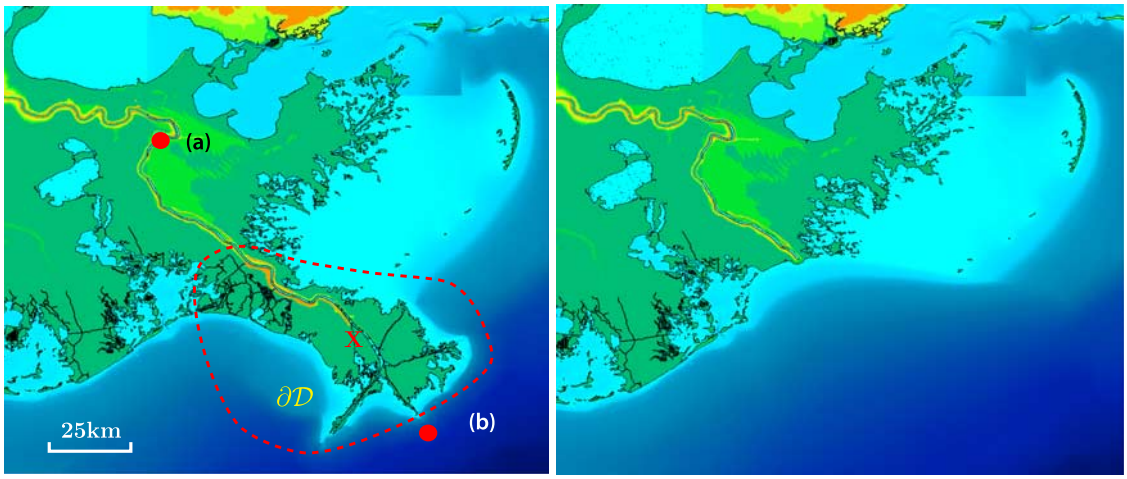

Figure 5. The topography of the coast of southern Louisiana (left) before and (right) after cutting the Balize Lobe. The actual course of the coastline is marked with a black line, and the boundary ∂D of the erased area is marked with a red dashed line. Within the erased region the elevation of the topography was calculated by solving Laplace's equation using Dirichlet boundary conditions with the values of the present elevation on ∂D. The locations of the two points which have been used for calculating the average slope are marked with red where point a has an elevation of about +5 m and point b has an elevation of around −60 m. Head of Passes is marked with a red cross; Tarbert Landing is outside the map.

A comparison of the two volumes in (11) and (14) confirms that the assumed long-term sediment supply $\overline{Q_s} = 214$ Mt/a and a retention fraction of 60–70% are good estimates during the Balize Lobe formation.

4.2. Comparison of Variables and Parameters With the Balize Lobe

[27] To rescale the variables and parameters of the model we ran a simulation with the model until a birdfoot delta was formed which visually compared well with the Balize Lobe of the Mississippi. The unitless horizontal resolution of the model was then isotropically rescaled by comparing the lattice spacing of the simulation grid with the real extent of the Balize Lobe. The simulation domain of 279 × 279 grid points corresponds to a square segment of the Mississippi Delta of about 110 km × 110 km ± 10 km. The river is running along the diagonal of the grid. The horizontal rescaled grid resolution is $r = r_x = r_y = 380 \pm 10$ m.

[28] The water inflow at the top of the delta I_0 is rescaled to match the long-term mean annual discharge $\overline{Q}$ with the scaling constant $c_I = 1 \times 10^8$ m^3/s then applied to all water fluxes I_{ij}. The rescaling of the water flux is necessary only to obtain the correct units in equation (4) as the model assumes steady state for the water flow in each time step. Similarly the sediment input at the top of the delta s_0 is rescaled to match the long-term mean annual sediment load $\overline{Q_s}$ with the scaling constant $c_s = 1 \times 10^4$ m^3/s then applied to all sediment fluxes J_{ij}. The rescaled variables and parameters are summarized in Table 1. We present ranges of the parameters which result from the uncertainties in the data.

[29] The rescaling factor for the elevation was obtained by comparing the highest and deepest points of the simulation domain with the DEM model. The slope of the simulation grid is given by the elevation difference between the upper left H_a and the lower right H_b corner divided by the length of the diagonal. Using the distance between the highest and lowest point of the simulation domain, $d = 150 \pm 5$ *km*, $H_a = 0.058$ and $H_b = -0.1$, we obtain a slope of $s = 0.8 - 1.4 \times 10^{-6}$. To obtain a comparable slope from the DEM model, we used the highest and lowest point in the chosen segment of the map outside of the deltaic deposits which are $z_{\max} = +5$ m (Figure 5, point a) close to New Orleans and $z_{\min} = -60 \pm 10$ m (see Figure 5, point b) on the sea side at the downstream end of the Balize Lobe. This yields an average slope of the Mississippi $s_{Miss} = 3.3 - 5.3 \times 10^{-4}$. As both slopes should be equal, all elevations of the simulation have to be rescaled by a factor of $c_h = 380 \pm 10$ m.

[30] As a consistency check, the rescaled lengths obtained by surface pattern comparison can now be used to compare the amount of subaqueous deposits in the delta region. The topography of the simulation data which corresponds to

Table 1. Rescaling of the Dimensionless Parameters in the Model for the Mississippi Birdfoot Delta

	Model	Rescaled Variable	Scaling constant
Horizontal scale	$\Delta x = 1$ gp $\Delta y = 1$ gp	$\Delta x' = r \cdot \Delta x$ $\Delta y' = r \cdot \Delta y$	$r = 370$–390 m/gp
Vertical scale	H_i V_i	$H_i' = c_h \cdot H_i$ $V_i' = c_h \cdot V_i$	$c_h = 370$–390 m
Time scale	$dt = 1$	$dt' = c_t \cdot dt$	$c_t = 950$–1150 s
Water flux	$I_0 = 1.7 \times 10^{-4}$ I_{ij} $I^\star$	$I_0' = c_I \cdot I_0$ $I_{ij}' = c_I \cdot I_{ij}$ $I^{\star\prime} = c_I \cdot I^\star$	$c_I = 1 \times 10^8$ m^3/s
Sediment flux	$s_0 = 2.5 \times 10^{-4}$ J_{ij}	$s_0' = c_s \cdot s_0$ $J_{ij}' = c_s \cdot J_{ij}$	$c_s = 1 \times 10^4$ m^3/s
Erosion-deposition rate	dS_{ij}	$dS_{ij}' = \epsilon dS_{ij}$	$\epsilon = \frac{r^2 c_h}{c_t} = 4.8$ $- 6.6 \times 10^4$ m^3/s
Erosion-deposition parameter	$c = 0.1$	$c' = \frac{\epsilon}{c_I}$ c	$c' = 4.8$ $- 6.6 \times 10^{-5}$

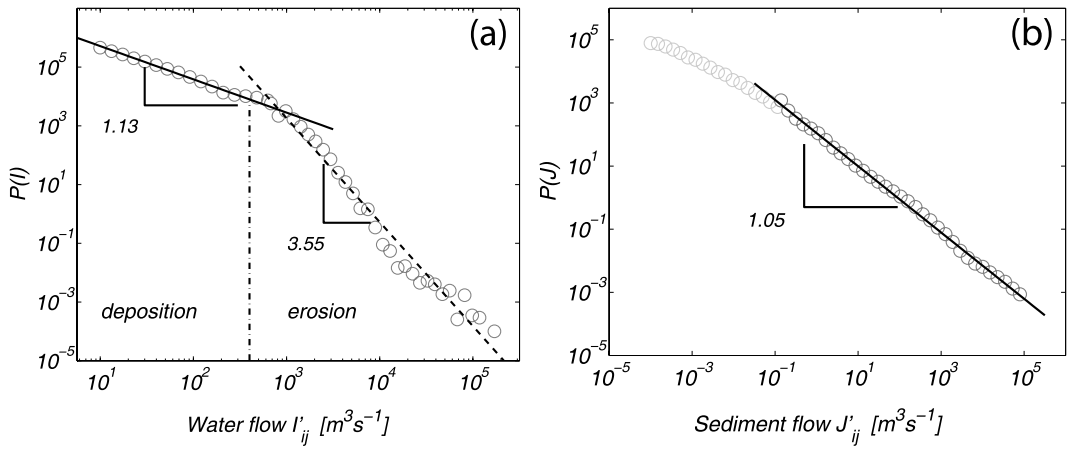

Figure 6. Histograms of (a) the magnitude of the water and (b) sediment flows in the deltaic plain integrated in space and time over the whole delta formation process. While the water flow shows a power law decay close to one (solid line) for small flows, the exponent for very large flows is 3.55 (dashed line) over almost 2 decades. The dotted vertical line corresponds to the current $I^\star$. The distribution of sediment flows shows a power law tail with exponent $\gamma = 1.0$ over 4 orders of magnitude. The solid black line shows a least squares fit of the tail (dark gray circles) to data.

today's Balize Lobe is calculated by subtracting the final simulated delta from the initial configuration. Using the rescaled variables one obtains a total deposited volume of

$$V_{\text{sim}} = 9.6 - 10.2 \times 10^{10}\, m^3 \tag{15}$$

which is very close to the values obtained from the Mississippi measurements. The rescaling factor for the time step in the model c_t comes from the age of the lobe τ. In the simulation a delta stage similar to today's Balize Lobe was obtained after 27 million steps which then yields a time resolution scaling constant $c_t = 1050 \pm 100$ s. From the modeled sediment flux we can estimate the sediment supply to the delta by integrating the fluxes over the age of the Balize Lobe using the sediment flux scaling factor (Table 1). Assuming the 60% sediment retention fraction we arrive at a simulated volume range identical to the flux-derived volume range in (11).

4.3. Erosion-Sedimentation Process

[31] The erosion-sedimentation rule in (4) is the fundamental equation in the model which drives delta formation. It was motivated by the approach of Foster and Meyer [*Foster and Meyer*, 1972], who proposed that the erosion/deposition rate should be proportional to the difference between the sediment transport capacity and the actual sediment load.

[32] The histogram of the flow current in Figure 6 shows that erosion will be the dominant process in the existing channels with a high flow rate, while deposition occurs over large areas of the forming lobe where $I_{ij} < I^\star$ and $I^\star = 4 \times 10^{-6}$ ($I^{\star\prime} = 400$ m^3/s). The parameter $I^\star$ is crucial for tuning the balance between these two processes. From Figure 6, it is noteworthy that the histograms of the water I_{ij} and the sediment J_{ij} fluxes follow a power law over a wide range of scales. This is indicative of the complex structure of the developing delta. The histograms (relative frequencies) of the model flow variables were obtained by integrating over time and space over the whole delta formation period. A similar behavior with fat tailed sediment flux distributions has been obtained by *Jerolmack and Paola* [2007] for avulsing rivers.

[33] The distribution of $dS^\star_{ij}$ is shown in Figure 7. Over the entire simulation domain the frequency of deposition $P(dS^\star > 0) = 0.0533$, was higher than that for erosion $P(dS^\star < 0) = 0.0071$. This confirms that deposition is the dominant process in the model. Integrated over the entire simulation time of the delta, erosion and deposition are concentrated only in nodes with water flow; therefore,

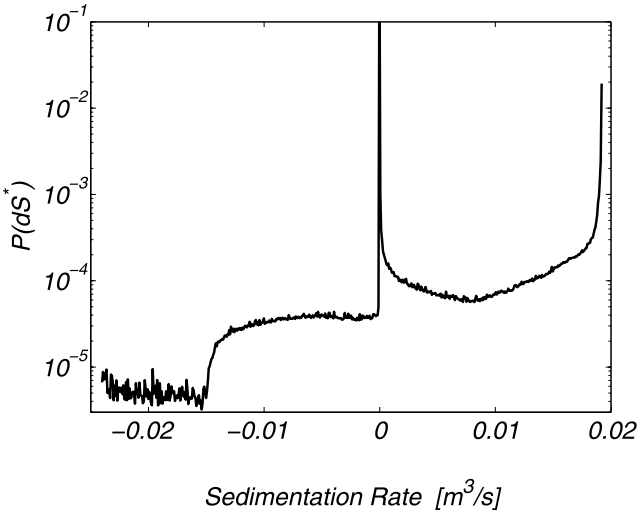

Figure 7. Relative frequency of the magnitude of the actual applied sedimentation-erosion rate $dS^\star$ averaged over time for the whole delta region. The strong peak at zero corresponds to the nodes with no flow (dry land). The value of the lower cutoff θ around -0.025 is outside of the range of the x axis.

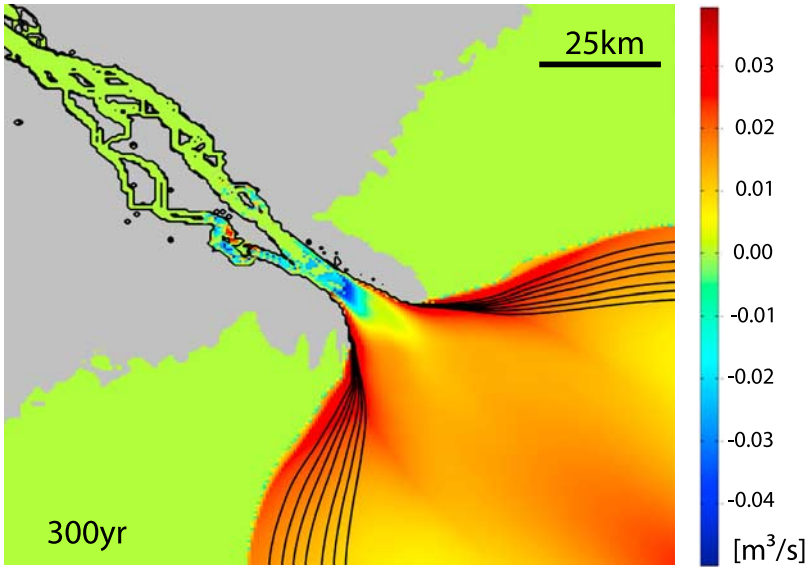

Figure 8. A combination of the two main aspects of the sedimentation and erosion process in the delta, which are (1) the sediment supply by the river, given by the contour levels (black) of the sediment flow, and (2) the erosion-sedimentation rate determined by the river current. The actual applied deposition rate is marked with the color range. The subaqueous deposition and the growth of the prodelta far beyond the actual mouth of the delta are clearly visible. Deltaic deposits form a complex subaqueous landscape with levees and bars confining the flow in the channel bed (compare to Figure 5).

$P(dS^\star = 0) = 0.9396$ is high. These are the cells where no erosion or deposition is taking place, either on the land or in the stable parts of the newly formed delta. The peak on the deposition side in Figure 7 corresponds to the deposition capacity $dS_{\max} = cI^\star$ in equation (5). Note that the infrequent high rates of erosion $dS < \theta$ are not actually applied in the model.

[34] When comparing the simulated water and sediment fluxes with observations it is important to recall that the model cannot resolve subgrid variability. The distribution channels in the Mississippi Delta are often narrower than the grid resolution $\Delta x'$ and are therefore more likely to have higher flow velocities and sediment transport. This phenomenon is common to all cellular river models [*Passalacqua et al.*, 2006].

[35] The delta formation process by erosion and deposition can be divided into several stages where each one is dominated by different effects. The early stage of the delta formation process is dominated by subaqueous deposition of sediment along the coast and the accumulation of a large amount of sediment on the continental shelf. Because of the high sediment supply by the river plume (Figures 4a and 4d) deposition also takes place far away from the river mouth leading to the accumulation of thick prodeltaic deposits which form the base of the future delta. Figure 8 shows the spatial distribution of the erosion-deposition process at the delta mouth after 300 years of delta progradation: Subaqueous mouth bars form in the model when the flow is diverging after the birdfoot lobe has prograded a certain distance into the sea, but they do not always become apparent above the water level.

[36] When the stream enters into deep ambient water the current is immediately decelerated leading to high deposition rates and fast subaqueous delta growth along the coast. In our simulation this effect can be observed in the early delta formation stages (Figures 4a and 4b) when the river enters into the sea where the conductivity σ_{ij} is much higher and the flow is distributed over a wider area. This leads to a decrease in the local water flow I_{ij} resulting in an increasing deposition rate. As there is still a slope in the direction of the main flow, the lateral deposition rate is slightly higher, forming subaqueous levees which confine the flow in the main channel direction. In general the morphodynamic feedback of the inflowing current leads to the formation of subaqueous landforms that confine the initial flow.

[37] The next phase is dominated by deposition in the channels and subaqueous sedimentation which leads to a more gradual transition from the river into the ocean. Channel deposition also limits the maximal distance a river channel segment can prograde before its slope becomes too shallow to transport sufficient sediment for further lobe growth. Strong deposition at the end of the channel head leads to a splitting of the stream, and subsequent overbank avulsion which causes lateral growth of the lobe. For the formation of a birdfoot delta it is important how the bank deposits force the channels to maintain their particular course by depositing levees along the channel. The formation of natural levees is inherent in our model as can be seen in Figure 9. As the lateral current in the model is much slower than the current in the direction of the main slope these flows lead to the deposition of levees confining the flow in the main direction.

[38] When the stream approaches the shoreline and deposits more sediment on the channel bed this sedimentation eventually overtops the levees, and overbank flow, rapid bank and channel bed aggradation, ultimately induce the failure of the natural levee forming a new outflow channel for the stream with a steeper slope. This phenom-

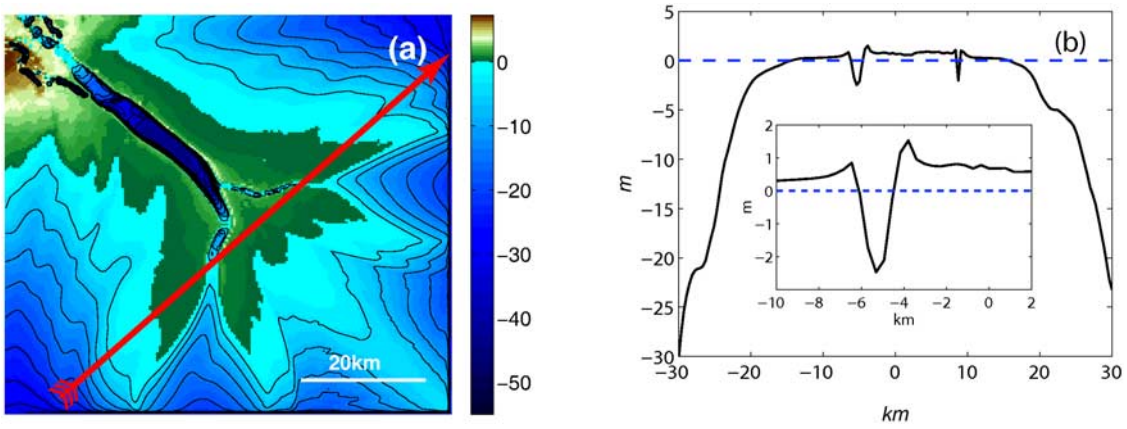

Figure 9. (a) Topography of the simulated delta lobe after 800 years. The contour lines of the subaqueous deposits are marked with black. (b) A cut through the delta lobe along the red arrow. The inset zooms into the area close to the south flowing channels where the levees can be clearly identified.

enon was observed several times during the simulation (Figures 4e and 4f). In literature this shift in the main sediment transporting channel is often referred to as type III lobe switching [*Coleman*, 1975]. A cut through the delta lobe after 27 million simulations steps, corresponding to about 800–1000 years, is shown in Figure 9. The subaerial part is quite flat and the channels are confined between natural levees Figure 9b, then the lobe drops quite steeply. The cut is indicated with a red line in Figure 9a. For comparison a cut through the Balize lobe of the Mississippi created from the bathymetry data (Divins and Metzger, 2006) is shown in Figure 10. The profile shows a morphology with steep drop-offs and a flat delta surface, similar to that in the simulation.

5. Long-Term Temporal Dynamics

[39] The different phases of the delta cycle can be identified in the time series of the land growth illustrated in Figure 11. There the change of the delta growth is plotted versus time. Formally the growth rate is defined as follows: Let N be all nodes on the lattice then the land/water fraction at a time t_k is defined by:

$$W(t_k) = \frac{\sum_{n=1}^{N} \Theta(H_i - V_i)}{N} \quad \text{where } \Theta(x) = \begin{cases} 0 & \text{if} x < 0 \\ 1 & \text{if} x \geq 0 \end{cases} \quad (16)$$

where N is the total number of all nodes in the lattice. Thus the growth rate is given by the difference $W(t_k) - W(t_{k-1})$.

[40] After a phase of constant growth, the stream breaks through the river banks and searches for a new path which is accompanied by high deposition and the formation of new subaerial delta parts corresponding to the peaks in Figure 11 (inset). When the shallow water behind the levee is filled up and the stream enters into deeper water the surface growth of the delta decreases tremendously. Subsequently the delta enters into a stage where a new subaqueous deposit is gradually built.

[41] Since the land formation process occurs in bursts, we investigate the possibility of temporal long range correlation of the delta growth. This can be characterized by the Hurst exponent H which was introduced by Hurst to describe the

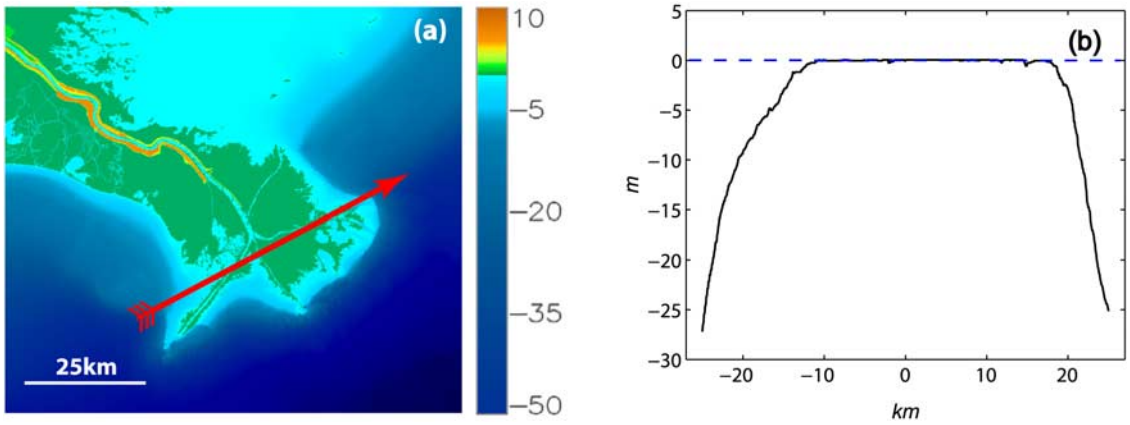

Figure 10. Cross section through the Mississippi Balize Lobe. (a) The cut is taken along the red arrow. The image and the cross section are based on the 3 arc sec DEM data of the coastal relief model (Divins and Metzger, 2006), where the land part does not resolve the depth of single channels which are definitely deeper than 5 m due to the fact that they are used as shipping waterways.

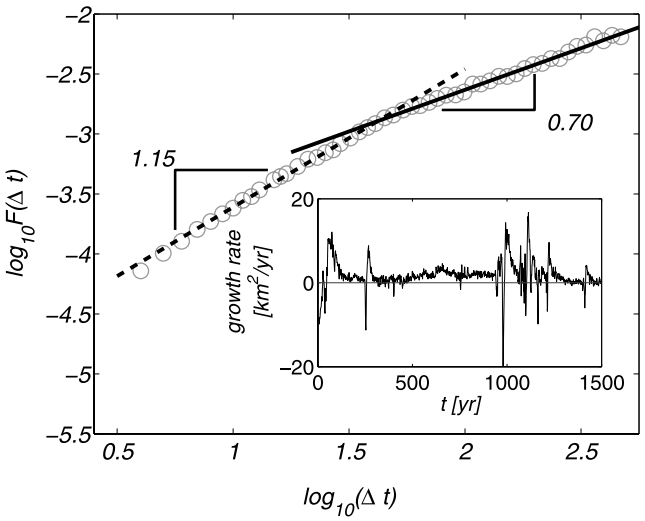

Figure 11. The inset shows the signal of the delta growth rate versus time, while the main plot is the corresponding DFA analysis averaged over 5 samples. The error bars of the sampling are not shown in the plot as they are smaller than the plot symbols. The straight lines are power law fits of $f \sim \Delta t^{\alpha}$ to the data with exponents $\alpha = 1.15$ (solid line) and $\alpha = 0.70$ (dashed line). The plot shows clearly two regimes with different exponents. For small time windows, delta growth is highly correlated, while on longer time scales the effects of the deltaic cycles average out. Note that the growth rate describes the change of the land-water surface fraction.

water level fluctuations of the Nile [*Hurst et al.*, 1965]. As a method to quantify the long-range correlation properties in a nonstationary time series we use detrended fluctuation analysis (DFA) [*Peng et al.*, 1994; *Hu et al.*, 2001; *Chen et al.*, 2002].

[42] Detrended fluctuation analysis is based on the computation of the scaling exponent H', which is equivalent to the Hurst exponent, by means of a modified mean square analysis. This method avoids the spurious long-range correlations due to nonstationary ties, by first integrating the data of the time series

$$y(k) = \sum_{i=1}^{k} [x(i) - M] \tag{17}$$

where $M = \frac{1}{k}\sum_{i=1}^{k} x(i)$ is the average value of the series $x(i)$ and k ranges between 1 and N. The time series $x(i)$ is the delta growth versus time during the formation of the birdfoot. Next, the time series is mapped onto a self affine stochastic process by dividing the integrated time series into K equally spaced intervals of length n. In each of these boxes a least squares fit (in our case linear) is performed on the data. The y coordinate of the resulting curve segments in box k then is called $y_n(t)$ where n denotes the length of the segment. In order to detrend the time series $y(t)$, the local trend $y_n(t)$ is subtracted in each of these boxes. Then the root mean square (RMS) fluctuation is calculated as,

$$F(n) = \sqrt{\frac{1}{N}\sum_{t=1}^{N} (y(t) - y_n(t))^2}. \tag{18}$$

Scaling is present if $F(n)$ has a power law dependence on the size of the time window n,

$$F(n) \propto n^{H'} \text{ for } n \to \infty, \tag{19}$$

where $H' \approx H$ asymptotically. The exponent H is related to the "$1/f$" noise spectral slope D_f (fractal dimension) by

$$D_f = 2H - 1. \tag{20}$$

It can be shown that in the case of no correlation, such as for example in a pure random walk, the exponent H is exactly 0.5. The range of the exponent for positively autocorrelated time series is $H > 0.5$. This means that if there is a trend to increase/decrease from time step t_{i-1} to t_i there is a higher probability to follow the trend than in a completely random process. A Hurst exponent of $H < 0.5$ will exist for a time series with antipersistent behavior (negative autocorrelation), which means that an increasing trend will be followed more probably by a decrease and vice versa. This behavior is sometimes called "mean reversion". To improve the statistics for the scaling exponent we have run 5 different realizations of the birdfoot delta formation with the same parameters but different seeds for the random numbers of the initial surface. For each sample the DFA analysis was performed and the averaged result is plotted in Figure 11. Two different correlation regimes can be clearly distinguished. On short time scales the land formation process is highly correlated with exponent $H = 1.2$, which corresponds to the formation of a new outflow channel and strong land growth. Over longer time windows the different cycles average out and yield a smaller exponent which was determined to be $H = 0.7$. We hypothesize that the stronger long-range correlations for shorter time scales is the result of the gradual lobe building phases at the mouths of the distributary channels, while at some temporal scale the random avulsion mechanisms lead to a breakdown of the correlation structure.

6. Conclusions

[43] Reduced complexity models have been shown to be a promising avenue in the geomorphological modeling of fluvial processes, being numerically simpler and more suitable for long-term simulation than their detailed fully physically based counterparts [e.g., *Brasington and Richards*, 2007; *Crave and Davy*, 2001; *Paola et al.*, 2001; *Murray and Paola*, 1994, 1997; *Van De Wiel et al.*, 2007].

[44] Recent applications of reduced complexity models to delta formation [*Sun et al.*, 2002; *Seybold et al.*, 2007] have shown that these models can capture the essence of delta formation mechanisms: the processes of transport, erosion and deposition of sediment by distributary channels. In this paper we go into more detail by applying one of these models [*Seybold et al.*, 2007] to the simulation of a real river-dominated delta, the Mississippi.

[45] The core of the model is the minimal hydrological model combined with an erosion/deposition law which although simple produces a plausible distribution of actual sedimentation rates. These rates should in principle be verifiable by measurements of deposition rates in the delta

from submarine cores. One of the main achievements of this model is that it generates subaerial and subaqueous channel and lateral levee formations and subaqueous profile morphology with steep drop-offs and flat delta surface which are similar to natural ones. In fact, the shape of the subaqueous part of the simulated delta compares very well with observations of the Mississippi delta derived from bathymetric data, which suggests that the sediment transport and deposition of sediment are captured well by the model.

[46] The dimensionless parameters of the original model were rescaled to match the formation of the most recent Balize Lobe of the Mississippi. Lattice dimensions were determined by scaling the geometry of the delta. Water and sediment inflow were scaled by the observed mean annual water and sediment fluxes measured at the upstream end of the delta. The modeling time step was scaled by the estimated age of the delta lobe. Mass consistency was checked by comparing the simulated and observed delta volumes determined from bathymetric data. The result is that the original dimensionless model formulation is cast in dimensional terms, which allows for a better appreciation of the process rates and the possibility to examine the scale dependence of parameters.

[47] The results also show that the simulated dynamics of the birdfoot delta growth have a characteristic time scale with a transition from a highly correlated regime for small time scales to a less correlated one at larger time scales. Delta growth in the model progresses in bursts, where a characteristic time scale separates periods of consistent delta growth by gradual sediment deposition at the mouths of distributary channels from periods within which random large-scale channel avulsions lead to rapid change and the formation of new channels and subaqueous-dominated deposition. We cannot of course verify these simulated temporal dynamics with observations of the Mississippi delta surface, but they do appear intuitively to be correct.

[48] Future work, apart from collecting data to verify the modeled process rates and time reconstructions in the Mississippi, should be aimed at examining the resolution dependence of the model parameters, their generality for river-dominated deltas, and the sensitivity of the results to the parameter set. The erosion/deposition law which, in the current model, is flow rate dependent and contains one parameter which represents both the erodibility of the surface and the trapping efficiency of fine material, may also be expanded by considering erosion and deposition separately, and adding information on grain size distributions and incipient motion thresholds.

[49] **Acknowledgments.** We would like to thank the referees and the editor for useful comments and suggestions. This work was funded by the Swiss National Science Foundation grant NF20021-116050/1, CNPq, CHPES, and FUNCAP.

References

Allen, G., D. Laurier, and J. P. Thouvenin (1981), Modern Mahakam Delta, Indonesia—Sand distribution and geometry in mixed tide and fluvial delta, *AAPG Bull.*, *65*(5), 889–889.

Bates, C. (1953), Rational theory of delta formation, *AAPG Bull.*, *37*(9), 2119–2162.

Brasington, J., and K. Richards (2007), Reduced-complexity, physically-based geomorphological modelling for catchment and river management, in *Geomorphology*, *90*, spec. issue, 171–177, doi:10.1016/j.geomorph.2006.10.028.

Chen, Z., P. C. Ivanov, K. Hu, and H. E. Stanley (2002), Effect of nonstationarities on detrended fluctuation analysis, *Phys. Rev. E*, *65*(4), 041107, doi:10.1103/PhysRevE.65.041107.

Coleman, J. (1975), *Deltas: Processes of Deposition and Models for Exploaration*, Contin. Educ., Champaign, Ill.

Coleman, J., and S. Gagliano (1964), Cyclic sedimentation in the Mississippi River Delta Plane, *Trans. Gulf Coast Assoc. Geol. Soc.*, *14*, 67–80.

Coleman, J., and S. Gagliano (1965), Sedimentary structures: Mississippi river deltaic plain, in *Primary Sedimentary Structures and Their Hydrodynamic Interpretation*, edited by G. V. Middleton, *Spec. Publ. Soc. Econ. Paleontol. Mineral.*, *12*, 133–148.

Coleman, J., and D. Prior (1980), *Deltaic Sand Bodies*, *Contin. Educ. Course Note Ser.*, vol. 15, Am. Assoc. Pet. Geol., Tulsa, Okla.

Corbett, D. R., B. McKee, and M. Allison (2006), Nature of decadal-scale sediment accumulation on the western shelf of the Mississippi River delta, *Cont. Shelf Res.*, *26*(17–18), spec. issue, 2125–2140, doi:10.1016/j.csr.2006.07.012.

Coulthard, T. J. (2001), Landscape evolution models: A software review, *Hydrol. Processes*, *15*(1), 165–173.

Coulthard, T. J., M. J. Kirkby, and M. G. Macklin (1998), Non-linearity and spatial resolution in a cellular automaton model of a small upland basin, *Hydrol. Earth Syst. Sci.*, *2*(2–3), 257–264.

Coulthard, T., D. Hicks, and M. V. D. Wiel (2007), Cellular modelling of river catchments and reaches: Advantages, limitations and prospects, *Geomorphology*, *90*(3–4), 192–207, doi:10.1016/j.geomorph.2006.10.030.

Crave, A., and P. Davy (2001), A stochastic "precipiton" model for simulating erosion/sedimentation dynamics, *Comput. Geosci.*, *27*(7), 815–827, doi:10.1016/S0098-3004(00)00167-9.

Davy, P., and A. Crave (2000), Upscaling local-scale transport processes in large-scale relief dynamics, *Phys. Chem. Earth, Part A*, *25*(6–7), 533–541, doi:10.1016/S1464-1895(00)00082-X.

Draut, A. E., G. C. Kineke, D. W. Velasco, M. Allison, and A. Prime (2005), Influence of the Atchafalaya River on recent evolution of the chenier-plain inner continental shelf, northern Gulf of Mexico, *Cont. Shelf Res.*, *25*(1), 91–112, doi:10.1016/j.csr.2004.09.002.

Edmonds, D. A., and R. L. Slingerland (2007), Mechanics of river mouth bar formation: Implications for the morphodynamics of delta distributary networks, *J. Geophys. Res.*, *112*, F02034, doi:10.1029/2006JF000574. (Correction, *J. Geophys. Res.*, 112, F03099, doi:10.1029/2007JF000874.)

Edmonds, D. A., and R. L. Slingerland (2008), Stability of delta distributary networks and their bifurcations, *Water Resour. Res.*, *44*, W09426, doi:10.1029/2008WR006992.

Fisk, H. (1947), Fine-grained alluvial deposits and their effects on Mississippi River activities, technical report, Miss. River Comm., U.S. Army Corps of Eng., Vicksburg, Miss.

Fisk, H. (1952), Geological investigation of the Atchafalaya Basin and the problem of Mississippi River diversion, technical report, Miss. River Comm., U.S. Army Corps of Eng., Vicksburg, Miss.

Fisk, H. G., and E. McFarlen Jr. (1955), Late Quaternary deltaic deposits of the Mississippi River—Local sediment and basin tectonics, in *Crust of the Earth, A Symposium*, edited by A. Poldervaart, *Spec. Pap. Geol. Soc. Am.*, *62*, 279–302.

Foster, G. R., and L. D. Meyer (1972), A closed-form erosion equation for upland areas, *Sedimentation: Symposium to Honor Prof. H. A. Einstein*, pp. 12.1–12.19, Colo. State Univ., Fort Collins.

Frazier, D. (1967), Recent deposits of the Mississippi River, their development and chronology, *Trans. Gulf Coast Assoc. Geol. Soc.*, *17*, 287–315.

Galloway, W. (1975), Process framework for describing the morphologic and stratigraphic evolution of deltaic depositional systems, in *Deltas*, edited by M. Broussard, pp. 87–98, Houston Geol. Soc., Houston, Tex.

Giosan, L., and J. Bhattacharya (Eds.) (2005), *River Deltas— Concepts, Models and Examples*, *Spec. Publ. Soc. Econ. Paleontol. Mineral.*, vol. 83, 508 pp., Tulsa, Okla.

Harris, C. K., P. A. Traykovski, and W. R. Geyer (2005), Flood dispersal and deposition by near-bed gravitational sediment flows and oceanographic transport: A numerical modeling study of the Eel River shelf, northern California, *J. Geophys. Res.*, *110*, C09025, doi:10.1029/2004JC002727.

Hoogendoorn, R., and G. Weltje (2006), A stochastic model for simulating long time series of river-mouth discharge and sediment load, in *Flooding in Europe: Challanges and Developments in Flood Risk Management*, edited by S. Begum and M. Stive, Springer, New York.

Hoyal, D. C. J. D., and B. A. Sheets (2009), Morphodynamic evolution of experimental cohesive deltas, *J. Geophys. Res.*, *114*, F02009, doi:10.1029/2007JF000882.

Hu, K., P. C. Ivanov, Z. Chen, P. Carpena, and H. Eugene Stanley (2001), Effect of trends on detrended fluctuation analysis, *Phys. Rev. E*, *64*(1), 011114, doi:10.1103/PhysRevE.64.011114.

Hurst, E., R. P. Black, and Y. M. Simaika (1965), *Long-Term Storage: An Experimental Study*, Constable, London.
Jerolmack, D., and C. Paola (2007), Complexity in cellular model river avulsion, *Geomorphology*, *91*(3–4), 259–270, doi:10.1016/j.geomorph.2007.04.022.
Keown, M. P., A. A. J. Dardeau, and E. M. Caussey (1986), Historic trends in the sediment flow regime of the Mississippi River, *Water Resour. Res.*, *22*(11), 1555–1564.
Kim, W., C. Paola, V. Voller, and J. Swenson (2006), Experimental measurement of the relative importance of controls on shoreline migration, *J. Sediment. Res.*, *76*(2), 270–283, doi:10.2110/jsr.2006.019.
Kolb, C. R., and J. van Lopik (1958), Geology of the Mississippi deltaic plain, southeastern Louisiana, technical report, Waterways Experiment Station, U.S. Army Corps of Eng., Vicksburg, Miss.
McFarlen, E., Jr. (1961), Radiocarbon dating of the late Quaternary deposits, south Lousiana, *Geol. Soc. Am. Bull.*, *72*, 129–158.
Morgan, J. (1977), *The Mississippi River Delta: Legal-Geomorphologic Evaluation of Historic Shoreline Changes*, *Geosci. Man*, vol. 16, Lousiana State Univ., Baton Rouge.
Mossa, J. (1996), Sediment dynamics in the lowermost Mississippi River, *Eng. Geol.*, *45*(1–4), 457–479, doi:10.1016/S0013-7952(96)00026-9.
Murray, A. (2003), Contrasting goals, strategies, and predictions associated with simplified numerical models and detailed simulations, in *Prediction in Geomorphology*, *Geophys. Monogr. Ser.*, vol. 135, edited by R. Iverson and P. Wilcock, pp. 151–165, AGU, Washington, D. C.
Murray, A. B. (2007), Reducing model complexity for explanation and prediction, *Geomorphology*, *90*, 178–191, doi:10.1016/j.geomorph.2006.10.020.
Murray, A., and C. Paola (1994), A cellular model of braided rivers, *Nature*, *371*, 54–57, doi:0.1038/371054a0.
Murray, A., and C. Paola (1997), Properties of a cellular braided stream model, *Earth Surf. Processes Landforms*, *22*, 1001–1025, doi:10.1002/(SICI)1096-9837(199711)22:11< 1001::AID-ESP798 > 3.0.CO;2-O.
Orton, G. J., and H. G. Reading (1993), Variability of deltaic processes in terms of sediment supply, with particular emphasis on grain size, *Sedimentology*, *40*(3), 475–512, doi:10.1111/j.1365-3091.1993.tb01347.x.
Overeem, I., and P. Sylvitski (2005), Three-dimensional numerical modeling of deltas, in *River Deltas—Concepts, Models and Examples*, edited by L. Giosan and J. Bhattacharya, *Spec. Publ. Soc. Econ. Paleontol. Mineral.*, *83*, 13–30.
Paola, C., et al. (2001), Exprimental stratigaphy, *GSA Today*, *11*(7), 4–9.
Passalacqua, P., F. Porté-Agel, E. Foufoula-Georgiou, and C. Paola (2006), Application of dynamic subgrid-scale concepts from large-eddy simulation to modeling landscape evolution, *Water Resour. Res.*, *42*, W06D11, doi:10.1029/2006WR004879.
Peng, C. K., S. V. Buldyrev, S. Havlin, M. Simons, E. H.. Stanley, and A. L. Goldberger (1994), Mosaic organization of dna nucleotides, *Phys. Rev. E*, *49*(2), 1685–1689, doi:10.1103/PhysRevE.49.1685.
Penland, S., J. R. Suter, and R. McBride (1987), Delta plain development and sea level history in the Terrebonne coastal region, Lousiana, in *Coastal Sediments*, pp. 1689–1705, Am. Soc. of Civ. Eng., Reston, Va.
Roberts, H. H. (1997), Dynamic changes of the Holocene Mississippi River delta plain: The delta cycle, *J. Coastal Res.*, *13*(3), 605–627.
Saucier, R. J. (1963), Recent geomorphic history of the Ponchartrain Basin, technical report, Lousiana State Univ., Baton Rouge.
Saucier, R. J. (1994), Geomorphology and Quaternary geologic history of the lower Mississippi valley, technical report, Miss. River Comm., Vicksburg.
Seybold, H., J. S. Andrade, and H. J. Herrmann (2007), Modeling riner delta formation, *Proc. Natl. Acad. Sci. U. S. A.*, *104*(43), 16,804–16,809.
Sheets, B., T. Hickson, and C. Paola (2002), Assembling the stratigraphic record: Depositional patterns and time-scales in an experimental alluvial basin, *Basin Res.*, *14*(3), 287–301, doi:10.1046/j.1365-2117.2002.00185.x.
Sun, T., C. Paola, G. Parker, and P. Meakin (2002), Fluvial fan deltas: Linking channel processes with large-scale morphodynamics, *Water Resour. Res.*, *38*(8), 1151, doi:10.1029/2001WR000284.
Swenson, J. B., C. Paola, L. Pratson, V. R. Voller, and A. B. Murray (2005), Fluvial and marine controls on combined subaerial and subaqueous delta progradation: Morphodynamic modeling of compound-clinoform development, *J. Geophys. Res.*, *110*, F02013, doi:10.1029/2004JF000265.
Syvitski, J. P. M., C. J. Vorosmarty, A. J. Kettner, and P. Green (2005), Impact of humans on the flux of terrestrial sediment to the global coastal ocean, *Science*, *308*(5720), 376–380, doi:10.1126/science.1109454.
Törnqvist, T., et al. (1996), A revised chronology for Mississippi River subdeltas, *Science*, *273*(5282), 1693–1696.
Van De Wiel, M. J., T. J. Coulthard, M. G. Macklin, and J. Lewin (2007), Embedding reach-scale fluvial dynamics within the caesar cellular automaton landscape evolution model, *Geomorphology*, *90*(3–4), 283–301, doi:10.1016/j.geomorph.2006.10.024.
van der Knijff, J., and A. de Roo (2008), Lisflood: Distributed water balance and flood simulation model, technical report, Eur. Union, Brussels.
Wolfram, S. (2002), *A New Kind of Science*, Wolfram Media, Champaign, Ill.
Wolinsky, M. A. (2009), A unifying framework for shoreline migration: 1. Multiscale shoreline evolution on sedimentary coasts, *J. Geophys. Res.*, *114*, F01008, doi:10.1029/2007JF000855.
Wright, L. D., and J. M. Coleman (1973), Variations in morphology of major river deltas as functions of ocean wave and river discharge regimes, *Am. Assoc. Pet. Geol. Bull.*, *57*(2), 370–398.

J. S. Andrade Jr., Departamento de Física, Universidade Federal do Ceará, 60451-970 Fortaleza, Ceará, Brasil. (soares@fisica.ufc.br)
H. J. Herrmann, H. J. Seybold, and H. M. Singer, Computational Physics for Engineering Materials, Institute for Building Materials, ETH Zurich, CH-8093 Zurich, Switzerland. (hans@ifb.baug.ethz.ch; hseybold@ethz.ch)
W. Kinzelbach and P. Molnar, Institute of Environmental Engineering, ETH Zurich, CH-8093 Zurich, Switzerland. (wolfgang.kinzelbach@ifu.baug.ethz.ch; peter.molnar@ifu.baug.ethz.ch)